Studies on the Catalysis of Carbon−Cobalt Bond Homolysis by Ribonucleoside Triphosphate Reductase: Evidence for Concerted Carbon−Cobalt Bond Homolysis and Thiyl Radical Formation†

Stuart S. Licht,‡ Squire Booker,‡,§ and JoAnne Stubbe*,‡,||

Departments of Chemistry and Biology, Massachusetts Institute of Technology, Cambridge, Massachusetts 02139

Received August 5, 1998; Revised Manuscript Received November 13, 1998

ABSTRACT: Ribonucleotide reductases (RNRs) catalyze the rate-determining step in DNA biosynthesis: conversion of nucleotides to deoxynucleotides. The RNR from *Lactobacillus leichmannii* utilizes adenosylcobalamin (AdoCbl) as a cofactor and, in addition to nucleotide reduction, catalyzes the exchange of tritium from [5′-^{3}H]-AdoCbl with solvent. Examination of this exchange reaction offers a unique opportunity to investigate the early stages in the nucleotide reduction process [Licht S. S., Gerfen, G. J., and Stubbe, J. (1996) *Science 271*, 477−481]. The kinetics of and requirements for this exchange reaction have been examined in detail. The turnover number for ^{3}H washout is 0.3 s^{-1}, and it requires an allosteric effector dGTP ($K_m = 17 \pm 3$ μM), AdoCbl ($K_m = 60 \pm 9$ μM) and no external reductant. The effects of active-site mutants of RTPR (C119S, C419S, C731S, C736S, and C408S) on the rate of the exchange reaction have been determined, and only C408 is essential for this process. The exchange reaction has previously been monitored by stopped-flow UV−vis spectroscopy, and cob(II)alamin was shown to be formed with a rate constant of 40 s^{-1} [Tamao, Y., and Blakley, R. L. (1973) *Biochemistry 12*, 24−34]. This rate constant has now been measured in D_2O, with [5′-$^2H_2$]-AdoCbl in H_2O, and with [5′-$^2H_2$]-AdoCbl in D_2O. A comparison of these results with those for AdoCbl in H_2O revealed k_H/k_D of 1.6, 1.7, and 2.7, respectively. The absolute amounts of cob(II)alamin generated with [5′-$^2H_2$]-AdoCbl in D_2O in comparison with AdoCbl in H_2O reveal twice as much cob(II)alamin in the former case. Similar transient kinetic studies with C408S RTPR reveal no cob(II)alamin formation. These experiments allow proposal of a minimal mechanism for this exchange reaction in which RNR catalyzes homolysis of the carbon−cobalt bond in a concerted fashion, to generate a thiyl radical on C408, cob(II)alamin, and 5′-deoxyadenosine.

The ribonucleoside triphosphate reductase (RTPR) of *Lactobacillus leichmannii* catalyzes the adenosylcobalamin (AdoCbl)-dependent reduction of nucleoside triphosphates to deoxyribonucleoside triphosphates (dNTP). The reducing equivalents are provided by a pair of cysteine residues (C419 and C119) in the enzyme's active site (*1*, *2*). Rereduction of the resulting cystine requires a second pair of cysteine residues (C731 and C736). These C-terminal cysteines can accept reducing equivalents from small organic dithiols or the thioredoxin (TR)/thioredoxin reductase (TRR)/NADPH reducing system to effect multiple turnovers (*3*). Ribonucleotide reduction also requires dNTPs as allosteric effectors with one binding site (*4*), controlling both substrate specificity and turnover rate. The fact that dNTPs are both products and allosteric effectors has made the steady-state (*5*) and transient-state (*6*) kinetic analysis of this system complex.

However, in addition to nucleotide reduction, RTPR also catalyzes an unusual reaction in which the 5′ hydrogens of AdoCbl exchange with the solvent (Scheme 1) (*7*, *8*). This reaction proceeds in the absence of nucleotide substrates, simplifying its kinetics relative to those observed for nucleotide reduction. We have recently proposed that this exchange reaction is an attractive model system for studying early events in catalysis (*2*). As shown in Scheme 1, these reactions are proposed to share a common intermediate: a protein-based thiyl radical residing on C408. The model postulates that the function of AdoCbl is to generate, in a concerted or stepwise fashion, this thiyl radical, 5′-deoxyadenosine (5′-dA), and cob(II)alamin. Generation of the thiyl radical in the absence of substrate can lead to the exchange of tritium from [5′-^{3}H]-AdoCbl by re-abstraction of hydrogen from 5′-dA in the course of the reversal of carbon−cobalt bond homolysis. Alternatively, in the presence of substrate, the thiyl radical initiates the nucleotide reduction process

† This research was supported by grants from the National Institutes of Health to J.S. (GM 29595). S.L. was a Howard Hughes Medical Institute Predoctoral Fellow.

* Corresponding author.

‡ Department of Chemistry.

§ Current address: Department of Biochemistry, University of Wisconsin, Madison.

|| Department of Biology.

[1] Abbreviations: RNR, ribonucleotide reductase; 5′-dA, 5′-deoxyadenosine; SF, stopped-flow; RFQ, rapid freeze quench; RTPR, ribonucleoside triphosphate reductase; AdoCbl, adenosylcobalamin; TR, thioredoxin; TRR, thioredoxin reductase; NADPH, β-nicotinamide adenine dinucleotide phosphate reduced form; dNTP, deoxyribonucleoside-5′-triphosphate; dGTP, 2′-deoxyguanosine-5′-triphosphate; EDTA, ethylenediaminetetraacetic acid; HEPES, 4-(2-hydroxyethyl)piperazine-1-ethanesulphonic acid; Ad, adenosine; RP, reverse-phase; wt, wild-type.

10.1021/bi981885i CCC: $18.00
Published on Web 01/05/1999

Scheme 1

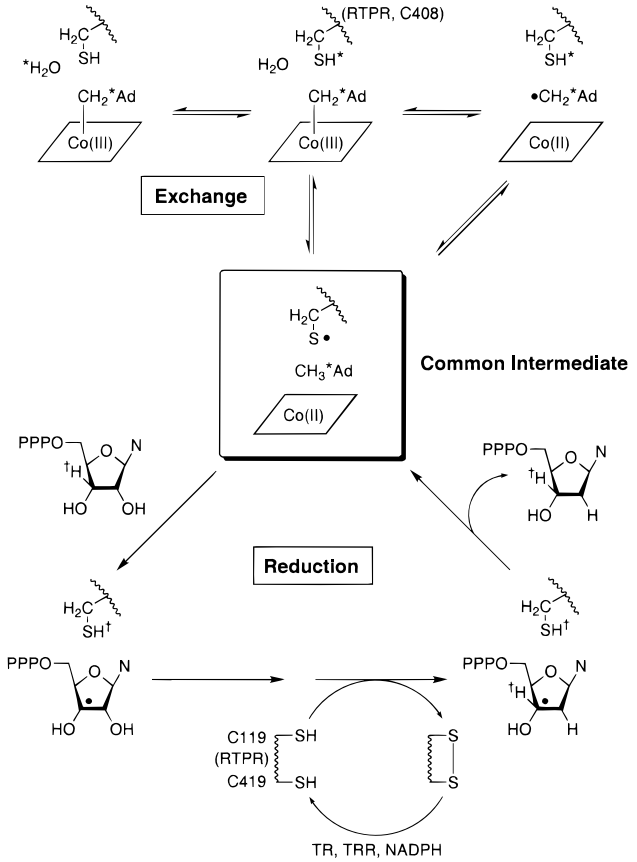

by 3′-hydrogen atom abstraction. After a complex set of transformations, hydrogen atom abstraction from the thiol group by a deoxynucleotide-based radical regenerates the thiyl radical.

Several experiments have provided evidence that the exchange reaction and nucleotide reduction share common intermediates. First, the exchange of tritium from [5′-^{3}H]-AdoCbl occurs with a k_{obs} of 0.3 s^{-1}. The rate constant for hydrogen exchange can be estimated to be ~10 s^{-1} by making the reasonable assumption of a selection effect of 10 on this process (due to the isotope effect on carbon−tritium bond cleavage) and a statistical correction of 3 (for the three hydrogens of the 5′-dA intermediate in this process). This rate constant is similar to that determined for nucleotide reduction (2 s^{-1}), making it likely that the exchange reaction is a mechanistically informative process.

Second, transient-state kinetic experiments have provided direct evidence that the exchange reaction and nucleotide reduction share common intermediates that are kinetically competent in their respective transformations (*6*, *9*, *10*). In the exchange reaction, both cob(II)alamin, monitored by stopped-flow (SF) UV−vis spectroscopy, and 5′-dA, monitored by rapid acid quench methods, are produced with observed rate constants of ~40 s^{-1} (*6*, *10*). Furthermore, rapid freeze quench (RFQ) EPR experiments (*9*, *10*) under identical conditions reveal an unusual paramagnetic species generated on the same time scale. A repetition of the RFQ EPR experiments using [β-$^2H_2$]-cysteine-labeled RTPR and simulation of the resulting spectra (*11*, *10*) indicate that the paramagnetic intermediate is a thiyl radical interacting with cob(II)alamin via exchange coupling and dipolar interactions.

Similar SF and RFQ experiments in the presence of substrate show that cob(II)alamin is formed with a k_{obs} > 200 s^{-1}. The observed paramagnetic species is almost identical to that observed in the absence of substrate. These studies thus suggest that information on the role of AdoCbl in thiyl radical formation, obtained by a detailed examination of the exchange reaction, is relevant to nucleotide reduction.

In the present paper, requirements for the exchange reaction have been identified and quantified. The effects of deuteration of the solvent and the cofactor ([5′-$^2H_2$]-AdoCbl) on the pre-steady-state kinetics of cob(II)alamin formation and on the amounts of cob(II)alamin formed have been determined. These studies provide additional support for the model in Scheme 1, and, in particular, for the importance of a thiyl radical in catalysis. The simplest interpretation of the reported isotope effect analysis is that this thiyl radial is generated by AdoCbl in a concerted fashion with formation of cob(II)alamin.

MATERIALS AND METHODS

General Methods. Nucleotides, nucleosides, and NADPH were obtained from Sigma. RTPR and mutant RTPRs were purified as reported (*12*). Wild-type (wt) RTPR has a specific activity of 1.4−1.5 μmol min^{-1} mg^{-1} using ATP as substrate. Prereduced and preoxidized RTPR were prepared as previously described (*13*). TR and TRR were purified as previously described (*14*, *15*). HPLC analyses were carried out on a Beckman Model 334 system. UV−vis spectroscopy was performed on a Cary 3 or Hewlett-Packard 8452A spectrophotometer. Scint-A scintillation fluid was obtained from Packard. Centricon-30 microconcentrators were obtained from Millipore. SF UV−vis experiments were carried out using an Applied Photophysics DX.17MV spectrophotometer. RFQ EPR experiments were carried out using an Update Instruments System 1000.

Synthesis of [5′-^{3}H]-AdoCbl. N^6-Benzoyl-2′,3′-O-isopropylidene adenosine (Ad) was prepared as reported (*16*). This was converted to N^6-benzoyl-2′,3′-O-isopropylidene Ad 5′-aldehyde via a Moffatt oxidation (*17*). The aldehyde hydrate was reduced with Na^3BH_4 (Dupont NEN, 500 μCi, 13.8 μCi/μmol) (*18*), and the benzoyl protecting group was removed using the method of Gaudemer et al. (*19*).

Deprotection of [5′-^{3}H]-2′,3′-O-isopropylidene Ad (160 mg) was achieved by dissolving it in 9:1 (v/v) H_2O/trifluoroacetic acid (10 mL) and stirring for 3.5 h. The solvent was then removed in vacuo leaving an oil, which was redissolved in 7:3 (v/v) methanol/H_2O. The solution was neutralized with 10 mL of Dowex AG 1-X2 (50−100 mesh, hydroxide form). The resin was washed with 1.1 L of 7:3 methanol/H_2O until all of the Ad had been removed as evaluated by A_{260}. The combined washings were pooled and concentrated in vacuo to give a white powder. The yield of [5′-^{3}H]-Ad was 94% (specific activity: 2×10^8 cpm/μmol).

[5′-^{3}H]-5′-Chloro-5′-dA was prepared from [5′-^{3}H]-Ad by reaction with thionyl chloride (*20*). [5′-^{3}H]-AdoCbl was prepared from [5′-^{3}H]-5′-chloro-5′-dA by reduction of hydroxocobalamin to cob(I)alamin, followed by nucleophilic displacement of the 5′-chloride (*19*). Partial purification of [5′-^{3}H]-AdoCbl was carried out by chromatography on

[2] S. Licht and J. Stubbe, unpublished results.

Dowex 50W X2. AdoCbl-containing fractions (as judged by UV−vis spectroscopy) were pooled, extracted into phenol, back-extracted into water, concentrated to 1−3.5 mM, and stored in foil-wrapped containers at −20 °C (*18*). The yield of [5′-^{3}H]-AdoCbl (specific activity 3.3 × 10^8 cpm/μmol) was 55 mg (5% from N^6-benzoyl-2′, 3′-isopropylidene Ad). The apparent increase in specific activity from [5′-^{3}H]-Ad to [5′-^{3}H]-AdoCbl is probably due to nonradioactive impurities in [5′-^{3}H]-Ad.

Purification of [5′-^{3}H]-AdoCbl. [5′-^{3}H]-AdoCbl (0.17 μmol) was purified directly before use by loading onto an Alltech C_{18} reverse-phase (RP) column equilibrated in 20% CH_3OH/80% H_2O. The column was washed in 20% CH_3OH/80% H_2O (flow rate 1 mL/min) for 10 min, followed by a linear gradient from 20% to 100% CH_3OH over 20 min, followed by isocratic elution for an additional 10 min with 100% CH_3OH. [5′-^{3}H]-AdoCbl eluted at 35 min (75% CH_3OH), with aquocobalamin and hydroxocobalamin eluting at 32 and 44 min (65 and 100% CH_3OH). [5′-^{3}H]-AdoCbl was diluted with cold material (final specific activity of 7 × 10^5−1 × 10^7 cpm/μmol) and concentrated to 1−2 mM.

Preparation of [5′-$^2H_2$]-AdoCbl. This material was prepared by a modification of the procedure of Hogenkamp et al. (*8*). The following components were combined in a final volume of 1 mL and lyophilized: 100 mM sodium dimethylglutarate (pH 7.3), 2 mM dGTP, 20 μM TR, 1.9 mM NADPH, and 24 nmol RTPR. The residue was dissolved in 1 mL of D_2O (99%), and TRR and AdoCbl (final concentrations of 1 μM and 100 μM, respectively) were added to start the reaction, which was incubated at 37 °C for 15 min. The solution was then loaded onto a C_{18} Sep-Pak (Millipore) and washed with water, and [5′-$^2H_2$]-AdoCbl was eluted with 100% methanol. The AdoCbl was then further purified by C_{18} RP-HPLC using a 10 min isocratic elution with H_2O, followed by a 30 min linear gradient to 100% MeOH (flow rate = 1.0 mL/min). The appropriate fractions were pooled, and the solvent was removed in vacuo.

[5′-$^2H_2$]-AdoCbl and unlabeled AdoCbl were characterized by electrospray mass spectrometry. The most abundant ion for AdoCbl, $[M + 2H]^{2+}$, has an *m*/*z* of 789.95 in good agreement with the calculated value of 790.33. [5′-$^2H_2$]-AdoCbl has an *m*/*z* of 790.93. The shift in *m*/*z* of one unit corresponds to a change of two mass units, since the charge of the ion is +2. A shoulder in the spectrum of the deuterated sample was observed at *m*/*z* 790.4 (a shift of one mass unit from the unlabeled material), accounting for ∼10% of the total abundance. This shoulder was assigned as the monodeuterated compound. Thus, the deuterated sample consists of 90% dideuterated AdoCbl and 10% monodeuterated AdoCbl, with an overall isotopic incorporation of 95%.

Assay for RTPR-Catalyzed Tritium Exchange from [5′-^{3}H]-AdoCbl. A typical assay contained in a volume of 305 μL: 50 mM potassium phosphate (pH 7.5) or 50 mM HEPES (pH 7.5), 300 μM dGTP, 4 mM EDTA, 50−300 nM wt RTPR (mutant concentrations were 12 μM C119S RTPR and 23 μM C419S RTPR), 50−200 μM [5′-^{3}H]-AdoCbl (7−100 × 10^5 cpm/μmol), 0.2 mM NADPH, 65 μM TR, and 0.5 μM TRR. All reagents except [5′-^{3}H]-AdoCbl and RTPR were preincubated at 37 °C for 3−5 min. After this preincubation, all manipulations except for scintillation counting were carried out in the dark under dim red light. [5′-^{3}H]-AdoCbl was added, and a 50 μL aliquot of the reaction mixture was removed and loaded onto a Sep-Pak C_{18} cartridge which had been previously washed with 10 mL of CH_3CN followed by 10 mL of H_2O. The cartridge was washed with 3 mL of H_2O, and a 1 mL aliquot of the eluate was analyzed by scintillation counting. The reaction was initiated by the addition of RTPR (5−10 μL) to the reaction mixture. At 1−2 min time intervals, 50 μL aliquots were removed and treated in the same manner as the zero time point. Rates of exchange were calculated from least-squares fits of plots of the amount of radioactivity (cpm) released to water versus time. As an internal check, the cofactor was isolated by washing each of the columns with 3 mL of CH_3CN, and a 1 mL aliquot was analyzed by scintillation counting.

For the determination of the K_m of AdoCbl, the reaction mixture was identical to that described above except that the concentration of AdoCbl was varied from 20 to 427 μM. For the determination of the K_m of dGTP, the concentration of dGTP was varied from 3 to 220 μM, with [AdoCbl] of 200 μM. Kinetic parameters were obtained by fits to the Michaelis−Menten equation (*21*).

Analysis for Consumption of Reductant during the Exchange Reaction. The reaction mixture was as described above except that the reaction volume was 500 μL, and unlabeled AdoCbl (120 μM) was employed. All components of the assay mixture, except RTPR, were placed in a 0.75 mL cuvette and incubated for 5 min at 37 °C. The cuvette was placed in the cell holder, and the background rate of NADPH oxidation was recorded at 340 nm. RTPR (1 μM) was added to the cuvette, and the enzyme-dependent rate of NADPH oxidation was subsequently measured. The net rate of NADPH oxidation was calculated as the difference between the observed rate and the background rate.

Deoxygenation of Solutions for Kinetic Experiments. The materials (0.5−2 mL) were placed in a septum-sealed 10 mL round-bottom flask equipped with a stirrer. If 100 μL or less was to be used, a septum-sealed Eppendorf tube was used, and the stirrer was omitted. The container was purged with argon (blown over the solution) for 20 min while stirring at 0 °C. All materials were transferred via a gastight Hamilton syringe. For SF experiments, the syringes and sample lines were filled with 50 mM dithionite 12 h prior to the actual experiments. They were then flushed with 20 mL of 0.2 M sodium dimethylglutarate, pH 7.3, which had been deoxygenated by bubbling argon through it for 2−3 h. Reaction mixtures were transferred to the loading syringes of the SF spectrophotometer via gastight syringe. Loading syringes, the windows of the drive unit, and exposed lines were covered in foil after addition of the reaction mixtures. Argon was bubbled through the bath that controlled the temperature of the sample holding unit for 3 h preceding data acquisition and throughout the course of the experiment.

Ability of Cysteine-to-Serine Mutants of RTPR to Catalyze Steady-State and Pre-Steady-State Cob(II)alamin Formation. The reaction mixture included in a final volume of 600 μL: 200 mM HEPES (pH 7.5), 50−60 μM AdoCbl, 0.12 mM TR, 1 μM TRR, 1 mM NADPH, and 70−75 μM C119S or C419S RTPR. This mixture was deoxygenated, and a 450 μL aliquot of the reaction mixture was transferred via a gastight syringe to a septum-sealed cuvette which had been purged with argon. The mixture was equilibrated at 37 °C. The UV−vis spectrum was recorded. To initiate the reaction,

a degassed solution of dGTP was added to a final concentration of 5 mM. Spectra were then recorded every 15 min for 75 min.

For SF studies under anaerobic conditions, 70 μM C419S RTPR or 70 μM C408S RTPR, 20 μM TR, 1 μM TRR, 2 mM NADPH, and 1 mM dGTP in 200 mM sodium dimethylglutarate, pH 7.3, were mixed with an equal volume of the same reaction buffer containing 100−110 μM AdoCbl and 1 mM dGTP, and the formation of cob(II)alamin was measured by monitoring the change of A_{525} at 37 °C.

Kinetic and Equilibrium Isotope Effects on Cob(II)alamin Formation Using [5′-$^1H_2$]- and [5′-$^2H_2$]-AdoCbl in H_2O and D_2O. To prepare 0.5 M dimethylglutarate buffer (pD 7.3), the acid was dissolved in D_2O and titrated to pH 6.9 using 5 N NaOD. For studies in D_2O, nonprotein components of the reaction mixture were lyophilized and redissolved in D_2O. RTPR (20−30 mg, ∼200 μL) was exchanged into D_2O by dilution into 2 mL of deuterated 5 mM sodium dimethylglutarate (pD 7.3) following concentration using a Centricon 30 apparatus. TR and TRR were exchanged the same way (∼50 μL of protein solution in ∼2 mL of deuterated buffer), except a Centricon 3 device was used. The total amount of H_2O introduced by this exchange procedure was calculated to be <5%. Reaction mixtures were deoxygenated by purging with D_2O-saturated argon.

RTPR (80−120 μM), 20 μM TR, 1 μM TRR, 2 mM NADPH, and 1 mM dGTP in 200 mM sodium dimethylglutarate, pH 7.3 (or pD 7.3), were mixed with an equal volume of the same reaction buffer containing 60−100 μM AdoCbl (or [5′-$^2H_2$]-AdoCbl) and 1 mM dGTP, and the formation of cob(II)alamin was measured by monitoring the change of A_{525} at 37 °C. Experiments with labeled and unlabeled coenzyme were carried out on the same day with the same batch of RTPR-containing reaction mixture.

To ensure that isotope effects were not due to the difference in pK_a between H_2O and D_2O, SF UV−vis experiments were also carried out at pH 6.9, the pH expected to be equivalent to a pD of 7.3 (*22*).

Kinetic Analysis. Fits to single or double exponentials were carried out using the least-squares fitting program included in the Applied Photophysics operating software or with Kaleidagraph. For a single exponential, traces were fit to the equation $A_t = A_\infty + C \exp(-kt)$, where A_t is the absorbance at time t, A_∞ is the final absorbance, C is the total absorbance change, and k is the observed rate constant; A_∞, C, and k are the adjustable parameters. For a double exponential, the equation used was $A_t = A_\infty + C_1 \exp(-k_1 t) + C_2 \exp(-k_2 t)$, where C_1 and C_2 are absorbance changes and k_1 and k_2 are rate constants.

Kinetic simulations were carried out using Hop*K*INSIM 1.3, a Macintosh version of KINSIM (*23*). Simulations used the experimentally determined concentrations of AdoCbl and RTPR as starting parameters so that small differences between experiments with isotopically labeled materials could be compared. The results of these simulations and the assumptions made are available in Supporting Information.

Global analysis was carried out using the program Dynafit.220 (*24*). Values for rate constants not involving the transfer of deuterium were obtained by global analysis of the kinetics of cob(II)alamin formation as a function of [AdoCbl] (*25*). A rapid equilibrium assumption for AdoCbl binding was made with a rate constant for the association of 10^8 M^{-1} s^{-1}. The dissociation rate constant was allowed to vary to obtain the equilibrium constant. To accommodate the rapid equilibrium assumption for thiyl radical formation in the stepwise mechanism, we set the rate constant for thiyl radical formation at 10^3 s^{-1} (∼10^2-fold greater than k_{obs}), and the rate constant for re-formation of thiol was allowed to vary to obtain the equilibrium constant. Exchange of the thiol with solvent was written as a second-order reaction of the enzyme with solvent (H_2O or D_2O), and the concentration of H_2O or D_2O was set at 55 M. Offsets of absorbance traces (i.e., the absorbance at time zero, which is subject to uncertainty due to the dead time of the instrument) and enzyme concentrations were allowed to vary to within 10% of their input values.

RESULTS

Requirements for the Exchange Reaction. Early studies of Hogenkamp and co-workers (*8*) reported that the exchange of tritium from [5′-^{3}H]-AdoCbl with solvent required the presence of reducing equivalents and an allosteric effector. They measured this reaction under a variety of conditions and observed maximum rates with 2 mM dGTP as an effector and 30 mM dihydrolipoate as a reductant. No rate constants were reported. In an effort to characterize quantitatively the requirements for the exchange reaction and to determine the appropriate conditions for pre-steady-state kinetic experiments, the K_m for AdoCbl and allosteric effector dGTP were measured at 37 °C. The results using TR, TRR, and NADPH as reductant and a standard kinetic analysis gave $K_{m,AdoCbl}$ of 60 ± 9 μM and a V_{max} of 0.3 μmol min^{-1} mg^{-1}. These values contrast with our recently determined constants for ATP reduction: 0.25 μM and 1.5 μmol min^{-1} mg^{-1}, respectively.

The $K_{m,app}$ for dGTP was determined to be 17 ± 3 μM in the presence of 200 μM AdoCbl. Saturating concentrations of AdoCbl were not used, as substrate inhibition was apparent at concentrations greater than 200 μM. The K_m for dGTP is 5-fold lower than the value of 100 μM previously reported (*8*). The differences may result from differences in buffer and reductant or from the method of their analysis, as they used only a single fixed time point assay.

While a reducing system was present in the determination of these kinetic parameters, our model in Scheme 1 suggests that external reductant should not affect the exchange rate, in contrast to the original report (*8*). Consistent with this model, the exchange reaction is not associated with the consumption of NADPH when the TR/TRR/NADPH reducing system is present (data not shown). To investigate the reductant dependence of the exchange reaction further, we measured it under a variety of conditions, and the results are summarized in Table 1. Studies with the prereduced RTPR revealed that it catalyzes this reaction at a rate that is ∼60% of that observed in the presence of the TR/TRR/NADPH reducing system. In fact, even oxidized RTPR, in which the active-site cysteines are present as a disulfide, is capable of carrying out this reaction (Table 1), although the rate is reduced ∼13-fold. These results establish that reductant is not required, but does affect the rate of the reaction.

The ability of the active-site cysteine mutants of RTPR to catalyze this reaction has also been examined. The model in Scheme 1 predicts that, of the five cysteines involved in

Table 1: Requirements for RTPR-Catalyzed Exchange of ^{3}H from [5′-^{3}H]-AdoCbl

	reductant	k (s^{-1})
wt RTPR		
prereduced	none	0.11
preoxidized	none	0.008
wt	TR/TRR/NADPH[a]	0.19
wt	DTT[b]	0.35
wt	dihydrolipoate[c]	0.33
mutant RTPRs		
C731S and C736S	TR/TRR/NADPH[a]	0.22
C119S	TR/TRR/NADPH[a]	0.001
C419S	TR/TRR/NADPH[a]	0.0035
C408S	TR/TRR/NADPH[a]	$<1.25 \times 10^{-5}$

[a] TR (65 μM), 0.5 μM TRR, 0.2 mM NADPH. [b] DTT (30 mM). [c] Dihydrolipoate (30 mM).

catalysis, only C408 should be essential for this process. In fact, our previous studies with this mutant indicated that these expectations are met, not only for the exchange reaction, but also for the nucleotide reduction process (*2*). The lower limit of detection for the exchange reaction was set at 1.25×10^{-5} s^{-1} by these studies. The studies with C419S and C119S RTPRs, in which the two cysteines delivering the reducing equivalents to generate deoxynucleotides are mutated, give rate constants of 0.0035 and 0.001 s^{-1} respectively, 1.5% and 0.5% of the rate catalyzed by wt RTPR (Table 1). These values are substantially lower than might have been expected from the model in Scheme 1, but well above the background rate observed with C408S RTPR. These cysteines are clearly not required for the exchange process, but their conformation appears to play a key role in determining the rate of this process. The recent structures of the R1 subunit of the *Escherichia coli* RNR in the oxidized and reduced states (*26*, *27*) show remarkable conformational flexibility of C462, corresponding to C419 in RTPR. This cysteine moves 6 Å relative to its position in the oxidized state. The similarities between the *Lactobacillus leichmannii* RNR and the *E. coli* RNR with respect to their interactions with the nucleotides of 2′-chloro-2′-deoxyuridine (*28*−*30*) and the unusual phenotypes of their cysteine to serine active-site mutants (*31*−*33*, *2*) suggest similarites in the secondary and tertiary structures of their active-site regions. Conformational flexibility corresponding to that observed with *E. coli* RNR would thus offer a reasonable explanation for the observed rates of exchange with these mutants.

The results with C736S and C731S RTPR mutants, in which the mutated cysteines are those that shuttle reducing equivalents in to and out of the active site via disulfide interchange from reductant TR or DTT, give rates almost identical to those observed with wt RTPR under identical conditions (*2*). This is the expected result given that neither of these mutants can produce dNTP using TR as a reductant, but that they have turnover numbers similar to wt RTPR when DTT is used as a reductant.

Finally, it is surprising from a chemical perspective that RTPR would catalyze thiyl radical/cob(II)alamin formation in the absence of substrate. One might have expected this process to be triggered by substrate binding, to avoid radical-mediated side reactions. However, a comparison of the K_m for AdoCbl (~60 μM) in the exchange reaction with that we measured in the reduction process (0.25 μM) may resolve this conundrum. Under physiological conditions, it could be

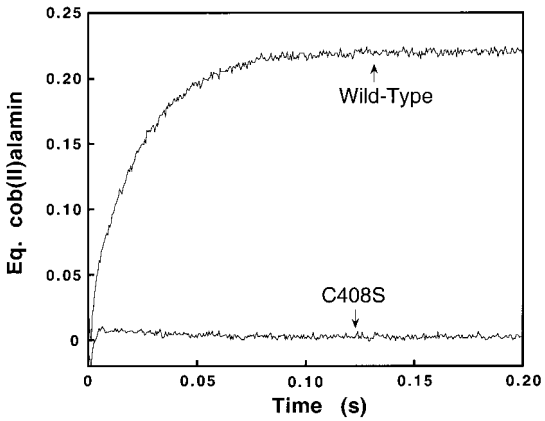

FIGURE 1: Effect of the C408S mutation on carbon−cobalt bond cleavage catalyzed by RTPR. C408S RTPR (70 μM), 20 μM TR, 1 μM TRR, 2 mM NADPH, and 1 mM dGTP in 200 mM sodium dimethylglutarate, pH 7.3, were mixed with an equal volume of the same reaction buffer containing 109 μM AdoCbl and 1 mM dGTP, and the formation of cob(II)alamin was measured by monitoring the change of A_{525} at 37 °C. The wt experiment was the same, with the exception that 100 μM wt RTPR was used. The solid traces show the equivalents of cob(II)alamin formed, calculated directly from the SF absorbance trace using the difference in extinction coefficients between AdoCbl and cob(II)alamin (4800 M^{-1} cm^{-1}).

that AdoCbl is never present in sufficiently high concentrations for the exchange reaction to compete with nucleotide reduction. The exchange reaction could thus be an artifact of our in vitro analysis conditions but, as outlined subsequently, one that closely mimics the early events in nucleotide reduction.

Ability of Mutant RTPRs to Catalyze C−Co Bond Homolysis. The two simplest mechanisms to account for the observed exchange reaction involve AdoCbl-mediated thiyl radical formation in a concerted or a stepwise process (Scheme 1) (*10*). Mutagenesis studies have suggested that C408 is the source of this thiyl radical. If thiyl radical formation occurs by a stepwise mechanism, mutation of C408 to serine would not be expected to prevent carbon−cobalt bond cleavage from occurring transiently. For a concerted formation of thiyl radical and cob(II)alamin, however, the difference in homolytic bond dissociation energies between O−H (119 kcal/mol) and S−H (88−91 kcal/mol) (*34*−*36*) might be expected to prevent such a reaction. C408S RTPR has therefore been examined by pre-steady-state SF UV−vis spectroscopy to determine its ability to catalyze transient formation of cob(II)alamin. The results of these experiments are shown in Figure 1. Monitoring at 525 nm (or from 465 to 535 nm) reveals no apparent absorbance change up to 200 ms, indicating that <0.01 equiv of cob(II)alamin (the lower limit of detection) is generated. Thus, either C408S RTPR is unable to catalyze transient carbon−cobalt bond cleavage, or if this cleavage occurs, re-formation of the carbon−cobalt bond occurs within the dead time of the instrument (<5 ms).

Similar pre-steady-state as well as steady-state experiments have been carried out with the C419S and C119S RTPRs. In the steady state, C119S gives no detectable change at 525 nm, while C419S gives rise to 0.36 equiv of cob(II)alamin after 1 h at 37 °C. This slow reaction is most likely analogous to the slow wt RTPR-mediated breakdown of AdoCbl shown by Yamada et al. to occur with a rate constant of 3×10^{-4}

s^{-1} ($t_{1/2}$ = 38 min) (*37*). Consistent with this interpretation is the observation that when C419S is mixed with AdoCbl in the presence of dGTP in the pre-steady state, <0.02 equiv of cob(II)alamin are formed. The inability to detect cob(II)alamin in the pre-steady state with either of these mutants is consistent with their slow exchange rates and suggests that these exchange rates result from an inability to cleave the carbon−cobalt bond efficiently.

Kinetic and Equilibrium Isotope Effects on Carbon−Cobalt Bond Homolysis. Kinetic and equilibrium isotope effects comparing rates and amounts of cob(II)alamin formed from [5′-$^1H_2$]-AdoCbl in H_2O with [5′-$^2H_2$]-AdoCbl in H_2O and D_2O have been carried out in an effort to distinguish between the concerted and stepwise models shown in Scheme 1 and eqs 1a and 1b

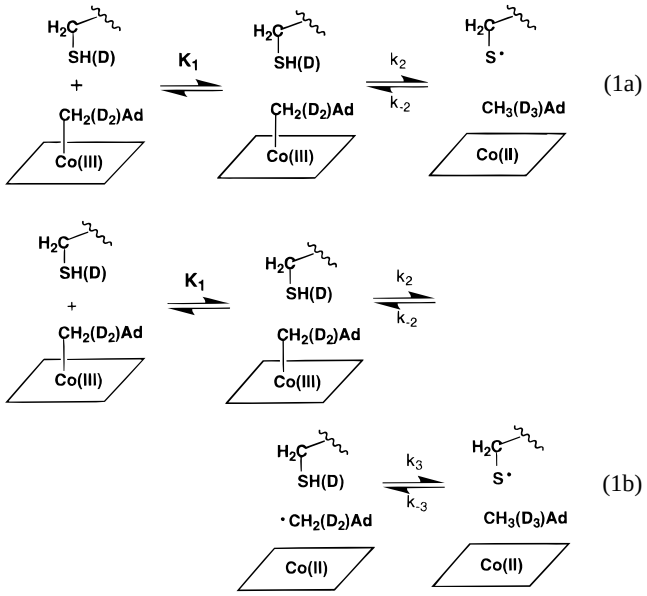

(1a)

(1b)

Initially, the rate of cob(II)alamin formation was measured with [5′-$^2H_2$]-AdoCbl in H_2O and compared to the results with unlabeled AdoCbl. Tamao and Blakley have previously reported a similar experiment using dihydrolipoate as a reductant and monitoring cob(II)alamin for only 200 ms (*6*). Fits of their data to a single exponential allowed them to report a k_H/k_D of 1.4. We have made a similar measurement using TR/TRR/NADPH as a reductant but have monitored the reaction for 5 s. The results are shown in Figure 2. What is strikingly evident, and not previously observed, is that at ~200 ms in the case of [5′-$^2H_2$]-AdoCbl, 35% more cob(II)alamin is observed than in the case of unlabeled AdoCbl. Cob(II)alamin then declines slowly from this maximum to give a concentration of cob(II)alamin identical to that observed in the all-protonated case. The data in the all-protonated case fit well to a single exponential, while that with [5′-$^2H_2$]-AdoCbl fit well to two exponentials: one associated with an increase in cob(II)alamin to a maximum (22 ± 2 s^{-1}) (k_1) and the other associated with a decrease in cob(II)alamin (1.3 ± 0.2 s^{-1}) (k_2). Comparison of the k_{obs} in the first case to k_1 in the second case gives an apparent $k_H/k_D = 1.7 \pm 0.2$ (Tables 2 and 3) similar to the number reported by Tamao and Blakely. This slow decline is most reasonably associated with exchange of the deuterium from AdoCbl with solvent. This rate constant can be compared with the rate constant for tritium washout from [5′-^{3}H]-AdoCbl of 0.3 s^{-1}, measured in either the pre-steady state or steady state (*2*, *10*).

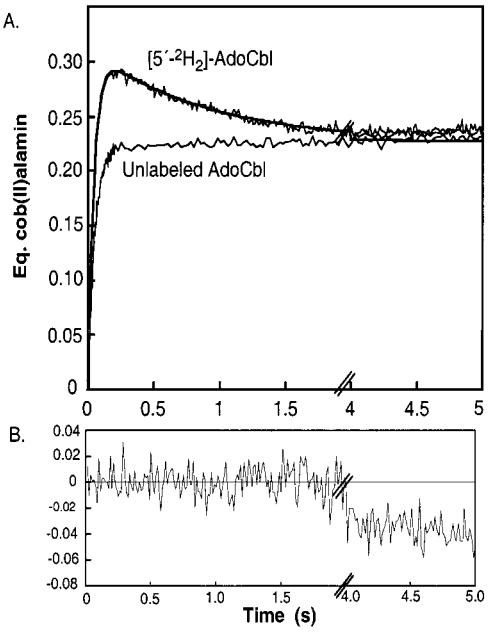

FIGURE 2: Kinetic isotope effect using [5′-$^2H_2$]-AdoCbl as cofactor. (A) A transient maximum in cob(II)alamin formation. Reaction conditions were as described in Figure 1, except 120 μM wt RTPR and 100 μM unlabeled AdoCbl or 80 μM [5′-$^2H_2$]-AdoCbl were used. The fit to a double exponential is superimposed (solid line) on the data for [5′-$^2H_2$]-AdoCbl. At longer times, a slower phase of cob(II)alamin formation becomes apparent. (B) Residuals for the reaction.

Table 2: Comparison of Experimental Results with Simulations[a]

		k_1 (s^{-1})	k_2 (s^{-1})	amp. 1 (equiv)	amp. 2 (equiv)
A. AdoCbl, H_2O	1	38 ± 4		0.23 ± 0.02	
	2	43		0.24	
	3	42		0.24	
B. [$^2H_2$]-AdoCbl, H_2O	1	22 ± 2	1.3 ± 0.2	0.32 ± 0.02	−0.09 ± 0.01
	2	37	0.5	0.3	−0.05
	3	27	0.6	0.38	−0.12
C. AdoCbl, D_2O	1	24 ± 2	1.0 ± 0.1	0.28 ± 0.02	0.13 ± 0.01
	2	45	1.0	0.21	0.08
	3	30	1.0	0.20	0.22
D. [$^2H_2$]-AdoCbl, D_2O	1	15 ± 1	0.5 ± 0.1	0.40 ± 0.03	0.04 ± 0.01
	2	27		0.29	
	3	12		0.36	

[a] 1 = experimental data, 2 = simulation of stepwise mechanism using HOPKINSIM, 3 = simulation of concerted mechanism using HOPKINSIM. Amplitudes are expressed as equivalents of cob(II)alamin. Final concentrations after mixing were the following: A, 60 μM RTPR, 50 μM AdoCbl, H_2O, similar k_1 (38 s^{-1}) and amplitude (0.19 equiv) were observed and simulated with 40 μM RTPR, 30 μM AdoCbl; B, 60 μM RTPR, 40 μM [5′-$^2H_2$]-AdoCbl, H_2O; C, 60 μM RTPR, 45 μM AdoCbl, D_2O; D, 40 μM RTPR, 30 μM [5′-$^2H_2$]-AdoCbl, D_2O.

To obtain further insight into the mechanism of the exchange reaction, the SF UV−vis experiments were next carried out in D_2O with AdoCbl and in D_2O with [5′-$^2H_2$]-AdoCbl and compared with the all-protonated case. The results of all of these experiments are summarized in Tables 2 and 3.

In D_2O with AdoCbl, the absorbance trace can be fit to two exponentials: one with a rate constant of 24 ± 2 s^{-1} accounting for 70% of the absorbance change and a second with a rate constant of 1.0 ± 0.1 s^{-1} accounting for the

Table 3: Summary of Observed and Predicted Isotope Effects

	k_{1H}/k_{1D}[a]	k_{1H}/k_{1D}[b]	k_{1H}/k_{1D}[c]
exptl data	1.7 ± 0.2	1.6 ± 0.2	2.7 ± 0.3
stepwise	1.2	1.0	1.5
concerted	1.5	1.4	3.1

[a] k_{1H}/k_{1D}; Ratio of rate constants obtained using AdoCbl versus [5′-^{2}H]-AdoCbl, both in H_2O, under comparable conditions (see Table 2). [b] k_{1H}/k_{1D}; Ratio of rate constants obtained using AdoCbl in H_2O versus D_2O, under comparable conditions (see Table 2). [c] k_{1H}/k_{1D}; Ratio of rate constants obtained using AdoCbl in H_2O versus [5′-^{2}H]-AdoCbl in D_2O, under comparable conditions (see Table 2).

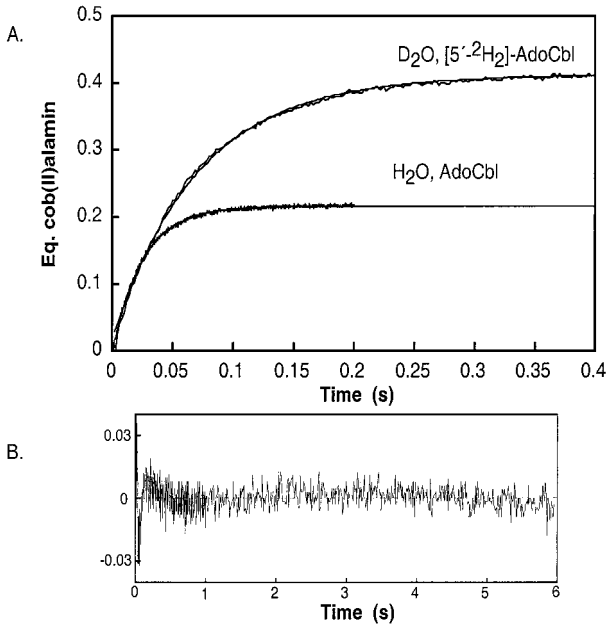

FIGURE 3: Equilibrium isotope effect observed with D_2O, [5′-$^2H_2$]-AdoCbl. (A) Kinetic traces. Reaction conditions were as described in Figure 1, except RTPR was 80 μM and AdoCbl (or [5′-$^2H_2$]-AdoCbl) was 60 μM. The trace for the D_2O, [5′-$^2H_2$]-AdoCbl experiment was fitted to a double exponential. (B) Residuals for the reaction.

remainder of the absorbance change (Table 2). Comparison of the rate constant for the first phase with that in H_2O gives an apparent solvent isotope effect of 1.6 ± 0.2. This isotope effect, as well as the others described later, was the same whether the all-protonated experiment was carried out at pH 7.3 or pH 6.9 (the pH equivalent to pD 7.3), thus ruling out the possibility that the pK_a difference between D_2O and H_2O is responsible for the observed effects (*22*). The second phase is associated with the wash-in of deuterium into the cofactor and hence an increase in cob(II)alamin. By 5 s, 0.36 equiv of cob(II)alamin is present. This number is identical (within experimental error) to that observed in the all-deuterium-labeled case.

When the reaction is carried out with [5′-$^2H_2$]-AdoCbl in D_2O, the resulting trace is also, unexpectedly, best fit to two exponentials (Figure 3) giving a k_1 of 15 ± 1 s^{-1} and a k_2 of 0.5 ± 0.1 s^{-1}. Comparison of the faster rate constant with that measured for AdoCbl in H_2O gives an apparent combined solvent and cofactor isotope effect of 2.7 ± 0.3 (Tables 2 and 3). In addition to the differences in rate of cob(II)alamin formation, D_2O also causes a dramatic perturbation of the amounts of cob(II)alamin formed relative to the amount in the all-protonated case (Figure 3). In the all-protonated case from 100 ms to 5 s, 0.2 equiv of cob(II)-alamin is present. In the all-deuterated case, the amplitude factors associated with the two phases are 0.4 and 0.04, respectively. The small amplitude factor associated with the unexpected second phase suggests that it results from our inability experimentally to make this system 100% deuterated.[3] The implications of these results in terms of the two mechanisms under consideration will be discussed subsequently.

A number of possible mechanisms can account for the shift in equilibrium in favor of cob(II)alamin in the totally deuterium-labeled system. The favored model is that this perturbation is associated with the influence that the low fractionation factor of sulfhydryl groups (*38*, *22*) has on the thiyl radical/thiol equilibrium. Fractionation factors of 0.4−0.6 of thiol groups indicate that transfer of deuterium from −SD to a group with fractionation factor ∼1 (e.g., a carbon center) is thermodynamically favorable (*39*).[4] Thus, according to our working model for the exchange mechanism in Scheme 1, deuteration of C408 should destabilize the thiol state of the enzyme relative to the state that contains the thiyl radical and cob(II)alamin, in which the deuterium is transferred to the methyl group of 5′-dA. Cob(II)alamin formation would therefore be more thermodynamically favorable in D_2O than in H_2O.[5]

Rapid Reversible Binding of AdoCbl to RTPR. The association and dissociation rates of substrate and cofactor binding to enzymes are often observed to be rapid compared to subsequent steps (*40*, *41*). When this is the case, kinetic modeling is simplified considerably. As a preliminary step toward the kinetic modeling required to distinguish between concerted and stepwise mechanisms (eqs 1a and 1b), we examined the kinetics of cob(II)alamin formation at low concentrations of AdoCbl and RTPR. If the association and dissociation rates are fast compared to the rate of carbon−cobalt bond cleavage, cob(II)alamin formation that follows monoexponential kinetics will be observed with no second kinetic phase. If the association and dissociation rates are slower than or comparable to the rate of carbon−cobalt bond cleavage, cob(II)alamin formation will exhibit a second kinetic phase corresponding to the approach to equilibrium of binding. This second kinetic phase will be more pronounced at low substrate concentrations, since the RTPR-AdoCbl association reaction is second-order (*41*).

Evidence to support the validity of the rapid equilibrium assumption was initially provided by the studies of Tamao and Blakley (*6*). They showed that rapid mixing of RTPR (∼10 μM), reductant, and dGTP with variable concentrations of AdoCbl (25 to 150 μM) and dGTP resulted in the formation of cob(II)alamin, with apparent first-order rate

[3] The [5′-$^2H_2$]-AdoCbl used was prepared by RTPR-catalyzed wash-in of deuterium from D_2O. The incorporation was ∼95% by atom, compared to ∼98% by atom for D_2O.

[4] The fractionation factor is defined as $(D/H)_{XL}/(D/H)_{L2O}$, where $(D/H)_{XL}$ and $(D/H)_{L2O}$ are the ratios of deuterium to hydrogen at equilibrium at the group of interest and the solvent, respectively. The fractionation factor for Co-CH_2R and H-CH_2R has not to our knowledge been measured.

[5] In fact, a true equilibrium between these species can never be obtained, for as outlined above, RTPR catalyzes a slow breakdown of AdoCbl ($t_{1/2}$ = 38 min). This rate is sufficiently slow, however, under the conditions examined, that a pseudo-equilibrium between these species can be measured. All subsequent sections refer to this pseudo-equilibrium as an equilibrium.

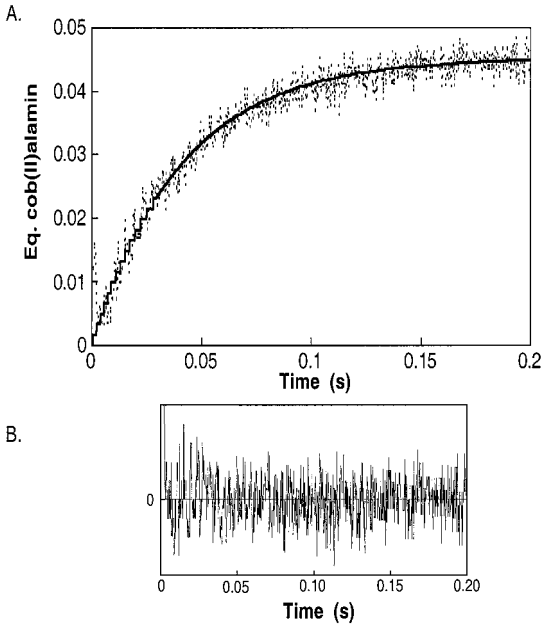

FIGURE 4: Cob(II)alamin formation is fitted well by a single exponential even at low [AdoCbl]. Reaction conditions were as described in Figure 1, except RTPR was 6 μM and AdoCbl was 24 μM. (A) Cob(II)alamin formation, fitted to a single exponential (solid line). (B) Residuals for the fit in A.

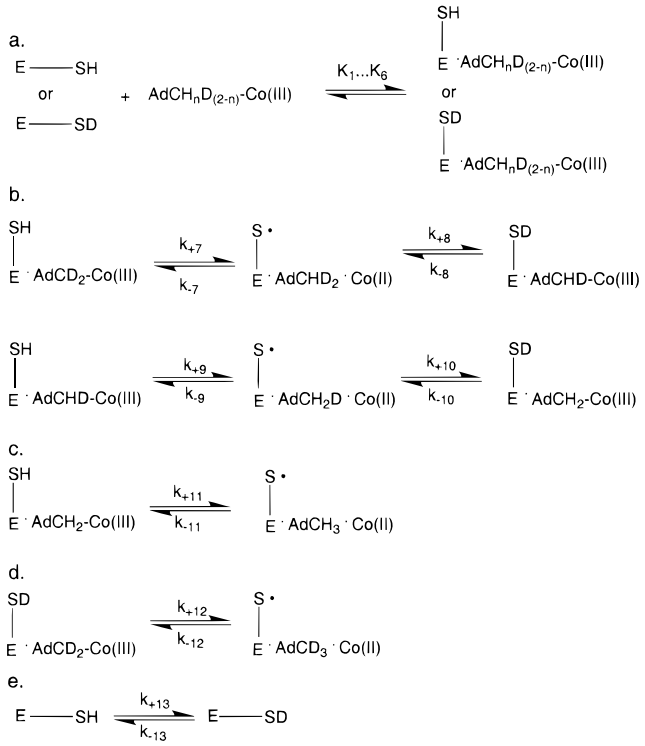

FIGURE 5: Concerted mechanism for the exchange reaction, treating isotopomers explicitly. Although this diagram depicts linear sequences of reactions, in the kinetic simulations equilibria were not treated as sequential: a, binding equilibria; b, carbon−cobalt bond cleavage and thiyl radical formation reactions with mixed isotopomers (i.e., containing both H and D); c, carbon−cobalt bond cleavage and thiyl radical formation reactions with H only; d, carbon−cobalt bond cleavage and thiyl radical formation reactions with D only; e, solvent exchange.

constants in the range 35−45 s^{-1}. At all concentrations of AdoCbl tested, the time dependence followed a single exponential. We have reproduced and extended these results. As shown in Figure 4, at 12 μM AdoCbl and 3 μM RTPR, the data are well-fit to a single exponential. Careful examination of the reaction time course did not reveal any second phase in the reaction kinetics at this or other low substrate concentrations examined.[6] The $t_{1/2}$ for approach to equilibrium for the binding reaction must therefore be small compared to the dead time of the instrument (3−5 ms), suggesting that the k_{obs} for binding is $\gg$200 s^{-1} (compared to k_{obs} of ~40 s^{-1} for cob(II)alamin formation). These data are thus consistent with the rapid equilibrium assumption.

The observation of monoexponential kinetics exhibiting no lag or burst phase over a range of [AdoCbl]s also has consequences for distinguishing between concerted and stepwise reactions.[6] The stepwise mechanism, which has two steps, can give rise to monoexponential kinetics only in certain special cases, the most probable of which is slow cob(II)alamin formation followed by rapid thiyl radical formation. The constraints that monoexponential kinetics put on the mechanistic possibilities will be examined in detail in the discussion.

Kinetic Modeling Using Experimental Data to Distinguish Between a Stepwise and a Concerted Mechanism. Simulations using Hop*K*INSIM 1.3 and global analysis using DynaFit.220 (*24*) were used in an effort to determine whether the experimental data monitoring cob(II)alamin formation can make a distinction between a concerted and a stepwise mechanism. A model for the concerted mechanism, including all of the different isotopomers of 5′-dA is shown in Figure 5. An analogous scheme for the stepwise mechanism is provided in Supporting Information (Figure S1). While the kinetic modeling is of necessity complex due to the mixture of isotopomers and consequently large number of unknowns, as evidenced in Figures 6 and 7 and Tables 2 and 3, the simulations are able to reproduce the experimental observations only in the case of the concerted model.

Initially, the simulations were carried out using HopKINSIM (*23*). The complexity of the mechanism (Figure 5) requires a number of simplifying and chemically reasonable assumptions. The details of the assumptions and the results are available in Supporting Information. The results favor the concerted over the stepwise model, Table 2.

Global analysis has also been used to determine the rate constants that provide a global best fit to all of the isotope effect data. In this case minimal assumptions have been made and hence this method serves as an additional check on the assumptions used in the numerical integration method. The global analysis method allows nonlinear least-squares regression analysis of an entire set of data simultaneously to find the parameters that best fit all of the data (*42*). Initially, the rate constants for the experiments with unlabeled cofactor and H_2O were determined by global fitting of SF traces obtained over a range of [AdoCbl]s (10−500 μM).[6] This method allowed direct determination of values for K_1, k_2, and k_{-2} (eq 1a). All of the rate constants involving transfer of deuterium were allowed to vary as adjustable parameters. Sets of data representing all four sets of isotopic conditions (AdoCbl with H_2O, [5′-$^2H_2$]-AdoCbl with H_2O, AdoCbl with D_2O, and [5′-$^2H_2$]-AdoCbl with D_2O) were fit simultaneously. A sampling of the fits to the data for the concerted

[6] The [AdoCbl] dependence of the kinetics of cob(II)alamin formation has been investigated in detail (*25*).

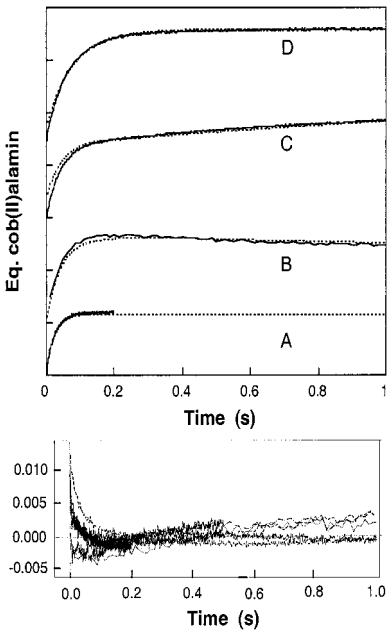

FIGURE 6: Global best fit of the concerted mechanism to pre-steady-state isotope effect data. The fits are shown as dashed lines: A, Unlabeled AdoCbl, H_2O (experimental conditions as in Figure 2); B, [5′-$^2H_2$]-AdoCbl, H_2O (experimental conditions as in Figure 2); C, AdoCbl, D_2O (experimental conditions as in Figure 3, except 60 μM AdoCbl was used in place of [5′-$^2H_2$]-AdoCbl); D, [5′-$^2H_2$]-AdoCbl, D_2O (experimental conditions as in Figure 3). Each tick mark represents 0.2 equiv of cob(II)alamin. Traces are shown offset from each other for clarity. The residuals are derived from the complete global analysis, which involved simultaneous fitting of seven traces.

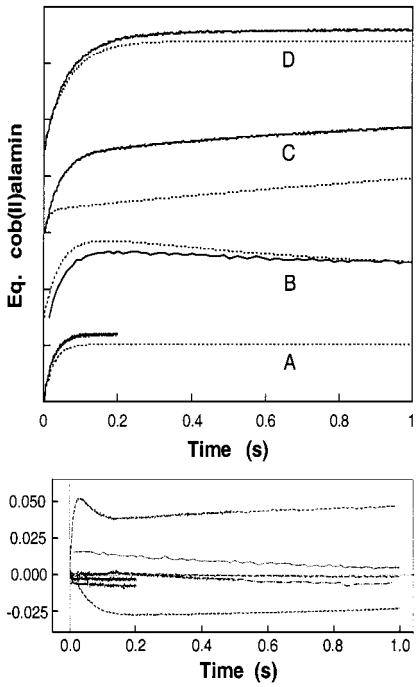

FIGURE 7: Global best fit of the stepwise mechanism to pre-steady-state isotope effect data. The fits are shown as dashed lines: A, unlabeled AdoCbl, H_2O (experimental conditions as in Figure 2); B, [5′-$^2H_2$]-AdoCbl, H_2O (experimental conditions as in Figure 2); C, AdoCbl, D_2O (experimental conditions as in Figure 3, except 60 μM AdoCbl was used in place of [5′-$^2H_2$]-AdoCbl); D, [5′-$^2H_2$]-AdoCbl, D_2O (experimental conditions as in Figure 3). Each tick mark represents 0.2 equiv of cob(II)alamin. Traces are shown offset from each other for clarity. The residuals are derived from the complete global analysis, which involved simultaneous fitting of seven traces.

mechanism are shown in Figure 6. The parameters associated with the best fits are summarized in Table 4.

Table 4 illustrates the rate constants obtained by global fitting of all of the isotopic experiments. Where "∼" are affixed, the microscopic rate constant obtained from the global fitting was associated with an error of 50−100%. Direct observation of the kinetics of isotopmer interconversion will be required to define these rate constants more precisely. The rate constants that can be derived from homoisotopic experiments alone (i.e., k_{+11}, k_{-11}, k_{+12}, k_{-12}) are the most precisely determined. Nevertheless, the results are in qualitative agreement with the values expected from statistical effects and chemically reasonable isotope effects. For example, comparing k_{-11} and k_{+10}, one would expect k_{+10} to be smaller by a factor of about 15, the product of a statistical factor of 3 (three hydrogens for k_{-11} vs one deuterium for k_{+10}), and an isotope effect of five (a value derived from the all-protonated vs all deuterated cases), in reasonable agreement with the observed values. The effects of isotopes on the equilibria are also roughly in agreement with expectations based on statistical and isotope effects. For example, the product of K_7 and K_8 should be the product of a statistical factor of 2 (deriving from the fact that the product of reaction 8 has two stereoisotopomers, while the reactant in reaction 7 has only one) and the fractionation factor (0.3 from the global analysis, 0.4−0.6 expected from model studies). Similarly, the product of K_9 and K_{10} should be one-half of the fractionation factor. While the error in the actual values is too large to interpret the comparison quantitatively, the actual values (∼1 and ∼0.1) follow the same trend as the expected values (0.6 and 0.15).

Table 4: Best-Fit Rate Constants for the Concerted Mechanism from Global Analysis[a]

K_1	4000 M^{-1}	k_{+9}	60 s^{-1}
K_2	4000 M^{-1}	k_{-9}	13 s^{-1}
K_3	4000 M^{-1}	k_{+10}	∼1 s^{-1}
K_4	4000 M^{-1}	k_{-10}	42 s^{-1}
K_5	4000 M^{-1}	k_{+11}	60 s^{-1}
K_6	4000 M^{-1}	k_{-11}	28 s^{-1}
k_{+7}	60 s^{-1}	k_{+12}	42 s^{-1}
k_{-7}	∼7 s^{-1}	k_{-12}	6 s^{-1}
k_{+8}	∼5 s^{-1}	k_{+13}	5 s^{-1}
k_{-8}	42 s^{-1}	k_{-13}	0 s^{-1}

[a] Rate constants are as defined in Figure 5. For simulation of reactions in H_2O, k_{+13} was 0 s^{-1} and k_{-13} was 5 s^{-1}.

The same procedure was used for fitting the same data to the stepwise mechanism (eq 1b, Figure 7, model Figure S1 in Supporting Information). For reasons discussed subsequently, thiyl radical formation was assumed to be much faster than carbon−cobalt bond homolysis and this step was modeled as a rapid equilibrium. The rate and equilibrium constants that best fit the experimental data with unlabeled cofactor and H_2O were determined by global fitting of the SF traces as described above.[6] Values for K_1, k_2, k_{-2}, k_3, and k_{-3} (eq 1b) were initially determined. With these rate constants fixed, the equilibrium constants involving transfer of deuterium were allowed to vary. The fits are shown in Figure 7, and the parameters describing the best fits are summarized in Supporting Information, Table S3. In several cases the fits do not define the parameters to within a factor of 2 (i.e., error >100%) and therefore no value is given.

Where the fits are associated with large uncertainties, the rate constant is preceded by an approximation sign (Table S3). The stepwise mechanism does not allow global fitting of all of the isotope effect data. None of the fits to the data are as good as for the concerted mechanism; see Figure 7 and Table 3. The failure of the fit to the experimental results is most clear in the experiments with unlabeled cofactor in D_2O (Figure 7C). The kinetic modeling using global analysis and the numerical integration methods (Supporting Information) are, therefore, most consistent with a concerted model, eq 1a.

EPR Evidence for the Nature of Paramagnetic Intermediates. EPR spectroscopy may also be useful in distinguishing between a stepwise and a concerted mechanism. In a stepwise mechanism, for example, 5′-dA• could be detectable as an intermediate if the rate of thiyl radical formation was sufficiently slow to allow its accumulation. RFQ-EPR experiments with [5′-$^2H_2$]-AdoCbl were therefore carried out to investigate this possibility. In agreement with previous studies (*9*), no perturbation of the EPR spectrum quenched at 28 ms (Supporting Information, Figures S4A and S4C) is apparent. Simulations of these spectra using a carbon-centered radical in place of a thiyl radical (as recently observed in the case of several AdoCbl-dependent enzymes that catalyze rearrangements) (*43*−*49*) indicate that, if the 5′-dA• were 10% of the observed paramagnetic species, it should have been detected. These results contrast with those from RFQ experiments carried out with RTPR in which all cysteines have been [β-$^2H_2$]-labeled (compare Figures S4A and S4B, Supporting Information), where a marked sharpening of hyperfine features associated with cob(II)alamin is detectable (*10*). These experiments are thus consistent with the hypothesis that 5′-dA• is not a required intermediate. The possibility of hydrogen atom transfer from C408 to a putative 5′-dA• during the freeze quenching process, or undetectable amounts of 5′-dA• with available methods, however, cannot be excluded.

DISCUSSION

Importance of C408 in the Exchange Reaction. Our model for the exchange reaction (Scheme 1) postulates a unique role for C408. Our detailed studies of this process (Table 1) using a variety of reductants and site-directed mutants support this proposal and eliminate previous proposals that invoked the requirement for and direct involvement of the reductant (*8*, *50*). Furthermore, these studies suggest that carbon−cobalt bond homolysis and formation of the thiyl radical are subtly dependent on the protein conformation, which in turn is influenced by active-site cysteine conformation and/or allosteric binding of reductant. The rate constants and requirements for the exchange process suggest, as we originally proposed (*10*), that it is an excellent model for the early stages in the nucleotide reduction process. Hence the detailed analysis of this simplified system was undertaken.

Equilibrium Solvent and Cofactor Isotope Effects as Evidence for a Thiyl Radical in the Exchange Reaction. Further evidence that supports the role of the thiyl radical in the exchange process comes from the observation that D_2O increases the amount of cob(II)alamin formed at equilibrium (Figure 3) by a factor of ∼2 relative to H_2O. The simplest explanation attributes this phenomenon to the low fractionation factor of 0.4−0.6 associated with thiols (*51*, *22*).

The hypothesis that this equilibrium effect arises from deuteration of C408 is also consistent with the unusual observation of a transient maximum in cob(II)alamin formation when [5′-$^2H_2$]-AdoCbl is studied in similar experiments (Figure 2). If C408 is relatively inaccessible to solvent, multiple cycles of carbon−cobalt bond cleavage/thiyl radical formation and carbon−cobalt bond re-formation/thiol regeneration could allow deuterium to fractionate between AdoCbl and the C408 thiol before the deuterium (or hydrogen) of C408 exchanges with the solvent. This fractionation process would initially favor formation of more thiyl radical and cob(II)alamin relative to the amount in the all-protonated case. As the deuterium is washed out, the amount of cob(II)alamin should and does return to an amount identical to that observed in the all-protonated case.

The observed increase in the amount of cob(II)alamin in the presence of [5′-^{2}H]AdoCbl or D_2O suggests that the residue that interacts directly with AdoCbl is a cysteine, consistent with the EPR data obtained by the RFQ method using isotopically [β-^{2}H]-cysteine-labeled RTPR (Figure S4, Supporting Information) (*10*). Furthermore, qualitatively similar inverse equilibrium isotope effects are observed in the presence of substrate,[2] suggesting that a thiyl radical is also an intermediate in nucleotide reduction, again in accord with freeze quench EPR results. Obtaining evidence for a thiyl radical intermediate from a continuous method carried out at a physiological temperature strongly supports the idea that this species is a true catalytic intermediate and not an artifact of the freeze quenching method.

Mechanism of Thiyl Radical Formation. Concerted versus Stepwise. The determination of whether steps in an enzymatic mechanism occur in a concerted or stepwise fashion is notoriously difficult. In fact, probes used to study this question often alter the mechanism under investigation. We have chosen to address this question using two methods: site-directed mutagenesis and isotope effects. The distinction between these mechanistic options is required for examining the thermodynamics of carbon−cobalt bond homolysis (accompanying manuscript) and understanding the observed rate acceleration of 10^{10} for the enzyme-catalyzed exchange reaction.

The concerted mechanism is appealing because it helps explain how RTPR catalyzes two thermodynamically unfavorable reactions. The homolytic bond dissociation energy of AdoCbl is reported to be ∼30 kcal/mol in solution (*52*, *53*), which makes carbon−cobalt bond cleavage very endergonic in a stepwise mechanism. However, coupling this step to C−H bond formation and S−H bond cleavage would be expected to reduce the enthalpic cost by ∼10 kcal/mol, since the homolytic bond dissociation energy of S−H is 88−91 kcal/mol, while that of C−H of a CH_3 is ∼100 kcal/mol (*34*−*36*). Similarly, coupling the thiyl radical's unfavorable re-abstraction of hydrogen from the methyl group of 5′-dA to carbon−cobalt bond re-formation would be expected to result in a net negative enthalpy change. This coupling is not possible in the stepwise mechanisms. The concerted reaction is similar to a well-characterized class of radical reactions described as molecule-induced homolyses. In these reactions homolytic cleavage of a non-radical species is

accelerated by interaction with another non-radical species (*54*, *55*).

The Inability of C408S RTPR to Catalyze Co−C Bond Cleavage is Consistent with a Concerted Mechanism. The observation that replacement of C408 with a serine, which makes hydrogen atom abstraction energetically unfavorable (O−H vs S−H, 120 vs 88−91 kcal/mol) also makes carbon−cobalt bond cleavage unfavorable suggests that these two reactions take place in a single step. Alternatively, this phenotype is consistent with a stepwise mechanism in which the first step (carbon−cobalt bond cleavage) is thermodynamically unfavorable, while the second step (thiyl radical formation) is thermodynamically more favorable and drives the reaction toward products.

This phenotype is furthermore inconsistent with two additional stepwise mechanisms: one in which the rate of carbon cobalt bond homolysis is greater than the rate of thiyl radical formation (case A) and one in which the rates are comparable (case B). Chemical precedent indicates that hydrogen abstraction from thiols by carbon-centered radicals occurs at $\sim 10^8$ M^{-1} s^{-1} (*56*), while thiyl radical abstraction of a hydrogen atom from 2-propanol occurs with a rate constant of $\sim 10^3-10^4$ M^{-1} s^{-1} (*57*). Thus, with even modest effective concentrations of ~1 M for 5′-dA• and thiyl radical at the active site of RTPR, the rate of approach to equilibrium would be $\sim 10^4-10^5$ s^{-1}, 10^2-10^3 faster than k_{obs} for cob(II)alamin formation. It is thus difficult to rationalize why the approach to equilibrium for a thermodynamically favorable hydrogen atom abstraction step in the stepwise mechanism would be slower than or comparable in rate to carbon−cobalt bond cleavage, unless a slow protein conformational change were required for this step to occur. However, if a conformational change were rate-limiting in thiyl radical formation, it would be difficult to explain the observed magnitude of the isotope effects (Tables 2 and 3), as there would be only a secondary isotope effect on carbon−cobalt bond homolysis and no isotope effect on thiyl radical formation. Thus, the inability to observe cob(II)alamin with C408S RTPR supports a concerted mechanism or a stepwise mechanism in which carbon−cobalt bond homolysis is slow and thiyl radical formation is rapid.

Additional arguments against a stepwise mechanism in which the rate constant for carbon−cobalt bond cleavage is greater than or equal to thiyl radical formation are provided by the observation that cob(II)alamin formation monitored in the pre-steady state occurs without any observable lag phase and is well-described by a single exponential (Figure 4). The stepwise mechanism case A predicts biphasic kinetics in which a burst followed by a slower increase in cob(II)alamin formation would be observed. Case B also predicts biphasic behavior, unless the rate constants for the two steps happen to be equal or very close to equal. Under conditions designed to maximize detection of two kinetic phases (i.e., low [AdoCbl] and [RTPR]), the data are best fit to a single exponential.

Finally, EPR evidence provides additional evidence against these two stepwise mechanisms (cases A and B). Both predict that 5′-dA• should be observable. However, RFQ EPR experiments carried out using [5′-$^2H_2$]-AdoCbl provide no evidence for its production (Figure S4, Supporting Information) (*9*, *10*). Given the experimental evidence and the chemical precedents, the most plausible possibility for the stepwise mechanism is thus the case in which hydrogen atom abstraction is much faster than cobalt−carbon bond homolysis and reformation. The remainder of the discussion will thus focus on making a distinction between the concerted case (eq 1a) and the stepwise case in which the first step is slow (eq 1b).

Solvent and Cofactor Kinetic Isotope Effects on Cob(II)alamin Make Distinct Predictions about Concerted and Stepwise Mechanisms. To make this distinction, kinetic isotope effects have been measured with [5′-$^2H_2$]-AdoCbl, D_2O, and both [5′-$^2H_2$]-AdoCbl and D_2O. Recall that the observed isotope effects are composites of forward and reverse rate constants and hence difficult to predict. The two mechanisms do, however, predict different isotope effects on microscopic steps, which in turn predict different observed kinetic and equilibrium isotope effects.

The stepwise mechanism (eq 1b) predicts a secondary kinetic isotope effect on k_2 and k_{-2} and an inverse equilibrium isotope effect (0.4−0.6) between 5′-dA• and the thiyl radical (*22*). A secondary isotope effect on k_2 would be expected to be normal and no greater than ~1.25 per deuterium (*39*), while that on k_{-2} would be expected to be inverse. These two steps in concert would not be expected to substantially alter the rate of approach to equilibrium. The equilibrium effect is thus likely to have the largest impact on the observed rate and equilibrium constants.

The concerted mechanism, in contrast, predicts primary isotope effects on both k_2 and k_{-2} (eq 1a). When deuterium is present on the thiol of C408, a primary kinetic isotope effect would be expected on k_2, and when deuterium is present at the 5′ position of 5′-dA, a primary kinetic isotope effect would be expected on k_{-2}. This mechanism, as with the stepwise mechanism, also predicts an inverse equilibrium isotope effect (K_2, eq 1a) of 0.4−0.6 due to the low fractionation factor of the thiol group (*22*). The magnitude of the observed isotope effect of 2.7 (Table 3) on cob(II)alamin formation in the all-protonated versus all-deuterated case thus favors a concerted model.

Global Analysis of Isotope Effect Data to Obtain Bests Fit Rate and Equilibrium Constants: Further Support for a Concerted Mechanism. Our simulations using HopKINSIM (Supporting Information) demonstrated that our isotope effect data could be modeled qualitatively to the concerted mechanism (eq 1a) with a small number of chemically reasonable assumptions. For the stepwise mechanism, however, a set of rate constants that both satisfied the initial assumptions and fit the data was not found. The uniqueness of the fits for the concerted mechanism is unknown, as is the question of whether acceptable sets of kinetic parameters actually exist for the stepwise mechanism. Global kinetic analysis methods have therefore been used to examine, with minimal assumptions, our ability to fit all of the isotope effect data quantitatively for the concerted and for the stepwise mechanisms.

The large number of isotopomers of 5′-dA (Figures 5 and S1 (Supporting Information)) complicates the analysis and makes it impossible to determine with high precision all of the rate constants in the mechanism using the data obtained to date. The presence of statistical effects also makes it difficult to determine accurately the true kinetic isotope effects on microscopic steps. However, despite this complexity, the modeling is able to reproduce, in the concerted case

only, the unusual isotope effects (Figures 2, 3, and 6 and Tables 3 and 4). Figure 6 shows remarkably good fits to the data under a variety of conditions. From these simulations with rate constants summarized in Table 4, the ratio of the kinetic constants for the all-protonated to all-deuterated case gives a kinetic isotope effect of 1.4 for carbon−cobalt bond homolysis/thiyl radical formation and 5 for carbon−cobalt bond re-formation/thiol regeneration. The ratio of these isotope effects gives a fractionation factor of 0.3, in reasonable agreement with the values of 0.4−0.6 measured in nonenzymatic systems (*22*) and used as a constraint in the HopKINSIM modeling.

As mentioned above, the major shortcoming of the experiments performed to date is that they do not give enough information to determine all of the microscopic rate constants, even in the concerted model. A modified concerted model in which statistical effects are built in as constraints would allow more precise determination of these constants using the data already obtained. Measurement of isotopic incorporation into 5′-dA and/or AdoCbl as a function of time and [AdoCbl] would determine microscopic rate constants more accurately. This could be achieved by rapid acid quench experiments, with mass spectrometric characterization of isotopic incorporation in 5′-dA and AdoCbl.

The stepwise mechanism, in contrast, fails to provide an acceptable global fit to the data (Figure 7 and Table S4, Supporting Information). The most dramatic deviations between experimental data and simulations are apparent in the cases of [5′-$^2H_2$]-AdoCbl in H_2O and with AdoCbl in D_2O (Figure 7B,C).

The global analysis of the isotope effect experiments thus supports the concerted mechanism over the stepwise mechanism. These experiments do not rule out 5′-dA• existing as a very high energy metastable intermediate rather than as a true transition state. However, the experiments described in this work argue that the potential energy surface describing the reaction is dominated by a single barrier.

Significance of a Concerted Mechanism For Carbon−Cobalt Bond Homolysis. A variety of kinetic experiments now support concerted formation of a thiyl radical in the exchange reaction. A concerted process would help to explain how the proposed mechanism for exchange could be accounted for thermodynamically. With such a mechanism, thermodynamically unfavorable steps such as carbon−cobalt bond homolysis and re-abstraction of hydrogen from 5′-dA by a thiyl radical are coupled to energetically favorable steps such as carbon−hydrogen bond formation and carbon−cobalt bond re-formation. This type of coupling, called molecule-induced homolysis, has long been known in free radical reactions (*54*, *55*). The concerted mechanism may thus help explain both rate acceleration by the enzyme and the remarkable perturbation of the thermodynamics of carbon−cobalt bond cleavage at the enzyme's active site. In addition, the unusual equilibrium isotope effect can be interpreted in the context of the concerted mechanism as arising from a low fractionation factor of the C408 thiol, thus corroborating the EPR evidence favoring a thiyl radical as a reaction intermediate.

With the establishment of a minimal chemical mechanism for the exchange reaction, further kinetic and thermodynamic analysis of this reaction becomes possible. The concerted mechanism argued for in this work forms the basis of a study of the thermodynamics and activation parameters of this reaction (*25*).

ACKNOWLEDGMENT

We thank Professor Morris Robins and Dr. Pamela England for advice on the synthesis of [5′-^{3}H]-AdoCbl. Mass spectrometric experiments were carried out in the laboratory of Prof. Klaus Biemann (Massachusetts Institute of Technology).

SUPPORTING INFORMATION AVAILABLE

Rate constants employed in the simulation of the concerted (Table S1) and stepwise (Table S2, Figure S1) mechanisms and the best-fit rate constants obtained for the stepwise mechanism by global analysis (Table S3), comparison of stepwise and concerted simulations with the experimental data for the reactions of RTPR with [5′-$^2H_2$]-AdoCbl in H_2O (Figure S2) and of [5′-$^2H_2$]-AdoCbl in D_2O (Figure S3), and effect of isotopic substitution of RTPR and AdoCbl on RFQ-EPR spectra (Figure S4) (15 pages). Ordering information is given on any current masthead page.

REFERENCES

1. Lin, A. I., Ashley, G. W., and Stubbe, J. (1987) *Biochemistry 26*, 6905−6909.
2. Booker, S., Licht, S., Broderick, J., and Stubbe, J. (1994) *Biochemistry 33*, 12679−12685.
3. Vitols, E., Hogenkamp, H. P. C., Brownson, C., Blakley, R. L., and Connellan, J. (1967) *Biochem. J. 104*, 58c−60c.
4. Chen, A. K., Bhan, A., Hopper, S., Abrams, R., and Franzen, J. S. (1974) *Biochemistry 13*, 654−661.
5. Vitols, E., Brownson, C., Gardiner, W., and Blakley, R. L. (1967) *J. Biol. Chem. 242*, 3035−3041.
6. Tamao, Y., and Blakley, R. L. (1973) *Biochemistry 12*, 24−34.
7. Beck, W. S., Abeles, R. H., and Robinson, W. G. (1966) *Biochem. Biophys. Res. Commun. 25*, 421−425.
8. Hogenkamp, H. P. C., Ghambeer, R. K., Brownson, C., Blakley, R. L., and Vitols, E. (1968) *J. Biol. Chem. 243*, 799−808.
9. Orme-Johnson, W. H., Beinert, H., and Blakley, R. L. (1974) *J. Biol. Chem. 249*, 2338−2343.
10. Licht, S., Gerfen, G. J., and Stubbe, J. (1996) *Science 271*, 477−481.
11. Gerfen, G. J., Licht, S., Willems, J.-P., Hoffmann, B. M., and Stubbe, J. (1996) *J. Am. Chem. Soc. 118*, 8192−8197.
12. Booker, S., and Stubbe, J. (1993) *Proc. Natl. Acad. Sci. U.S.A. 90*, 8352−8356.
13. Booker, S. (1994) Ph.D. Thesis, Massachusetts Institute of Technology.
14. Lunn, C. A., Kathju, S., Wallace, C., Kushner, S., and Pigiet, V. (1984) *J. Biol. Chem. 259*, 10469−10474.
15. Russel, M., and Model, P. (1985) *J. Bacteriol. 163*, 238−242.
16. Jenkins, I. D., Verheyden, J. P. H., and Moffatt, J. G. (1976) *J. Am. Chem. Soc. 98*, 3346−3357.
17. Ranganathan, R. S., Jones, G. H., and Moffatt, J. G. (1974) *J. Org. Chem. 39*, 290−298.
18. Gleason, F. K., and Hogenkamp, H. P. C. (1971) *Methods Enzymol. 18C*, 65−71.
19. Gaudemer, A., Zylber, J., Zylber, N., Baran-Marszac, M., Hull, W. E., Fountoulakis, M., König, A., Wölfle, K., and Rétey, J. (1981) *Eur. J. Biochem. 119*, 279−285.
20. Robins, M. J., Hansske, F., Wnuk, S. F., and Kanai, T. (1991) *Can. J. Chem. 69*, 1468−1474.
21. Cleland, W. W. (1979) *Methods Enzymol. 63*, 103−138.
22. Schowen, K. B., and Schowen, R. L. (1982) *Methods Enzymol. 87*, 501−606.

23. Barshop, B. A., Wrenn, R. F., and Frieden, C. (1983) *Anal. Biochem. 130*, 134−145.
24. Kuzmic, P. (1996) *Anal. Biochem. 237*, 260−273.
25. Licht, S. S., Lawrence, C. C., and Stubbe, J. (1999) *Biochemistry 38*, 1234−1242.
26. Uhlin, U., and Eklund, H. (1994) *Nature 370*, 533−539.
27. Eriksson, M., Uhlin, U., Ekberg, M., Regnstrom, K., Sjoberg, B., and Eklund, H. (1997) *Structure 5*, 1077−1092.
28. Harris, G., Ator, M., and Stubbe, J. (1984) *Biochemistry 23*, 5214−5225.
29. Ator, M. A., and Stubbe, J. (1985) *Biochemistry 24*, 7214−7221.
30. Ashley, G. W., Harris, G., and Stubbe, J. (1988) *Biochemistry 27*, 4305−4310.
31. Mao, S. S., Holler, T. P., Bollinger, J. M., Yu, G. X., Johnston, M. I., and Stubbe, J. (1992) *Biochemistry 31*, 9744−9751.
32. Mao, S. S., Holler, T. P., Yu, G. X., Bollinger, J. M., Booker, S., Johnston, M. I., and Stubbe, J. (1992) *Biochemistry 31*, 9733−9743.
33. Mao, S. S., Yu, G. X., Chalfoun, D., and Stubbe, J. (1992) *Biochemistry 31*, 9752−9759.
34. Benson, S. W. (1978) *Chem. Rev. 78*, 23−35.
35. McMillen, D. F., and Golden, D. M. (1982) *Annu. Rev. Phys. Chem. 33*, 493−532.
36. Griller, D., and Martinho Simoes, J. A. (1990) *Sulfur-Centered Reactive Intermediates in Chemistry and Biology* (Chatgilialoglu, C., and Asmus, K.-D., Eds.) Plenum Press, New York.
37. Yamada, R., Tamao, Y., and Blakley, R. L. (1971) *Biochemistry 10*, 3959−3968.
38. Lienhard, G. E., and Jencks, W. P. (1966) *J. Am. Chem. Soc. 88*, 3982−3995.
39. Cleland, W. W. (1987) *Secondary and Solvent Isotope Effects* (Buncel, E., and Lee, C. C., Eds.) Elsevier, Amsterdam, The Netherlands.
40. Fersht, A. R. (1985) *Enzyme Structure and Mechanism*, W. H. Freeman & Co., New York.
41. Johnson, K. A. (1992) *The Enzymes* (Sigman, D. S., Ed.) Academic Press, San Diego, CA.
42. Beechem, J. M. (1992) *Methods Enzymol. 210*, 37−54.
43. Michel, C., Albracht, S. P. J., and Buckel, W. (1992) *Eur. J. Biochem. 205*, 767−773.
44. Keep, N. H., Smith, G. A., Evans, M. C. W., Diakun, G. P., and Leadlay, P. F. (1993) *Biochem. J. 295*, 387−392.
45. Zelder, O., Beatrix, B., Leutbecher, U., and Buckel, W. (1994) *Eur. J. Biochem. 226*, 577−585.
46. Zhao, Y., Abend, A., Kunz, M., Such, P., and Rétey, J. (1994) *Eur. J. Biochem. 225*, 891−896.
47. Beatrix, B., Zelder, O., Kroll, F. K., Örlygsson, G., Golding, B. T., and Buckel, W. (1995) *Angew. Chem., Int. Ed. Engl. 34*, 2398−2401.
48. Padmakumar, R., and Banerjee, R. (1995) *J. Biol. Chem. 270*, 9295−9300.
49. Bothe, B., Darley, D. J., Albracht, S. P. J., Gerfen, G. J., Golding, B. T., and Buckel, W. (1998) *Biochemistry 37*, 4105−4113.
50. Ong, S. P., Nelson, L. S., and Hogenkamp, H. P. C. (1992) *Biochemistry 31*, 11210−11215.
51. Jencks, W. P. (1969) *Catalysis in Chemistry and Enzymology*, Dover, New York.
52. Finke, R. G., and Hay, B. P. (1984) *Inorg. Chem. 23*, 3041−3043.
53. Halpern, J., Kim, S.-H., and Leung, T. W. (1984) *J. Am. Chem. Soc. 106*, 8317−8319.
54. Walling, C., Heaton, L., and Tanner, D. D. (1965) *J. Am. Chem. Soc. 87*, 1715.
55. Pryor, W. A. (1966) *Free Radicals*, McGraw-Hill, New York.
56. Akhlaq, M. S., Al-Baghdadi, S., and von Sonntag, C. (1987) *Carbohydr. Res. 164*, 71−83.
57. Schöneich, C., Bonifacic, M., and Asmus, K.-D. (1989) *Free Radical Res. Commun. 6*, 393−405.

BI981885I